



Numerical modeling of the plasma plume propagation and oxidation during pulsed laser deposition of complex oxide thin films

T. Wijnands, E. P. Houwman , G. Koster, G. Rijnders, and M. Huijben*
MESA+ Institute for Nanotechnology, University of Twente, 7500 AE Enschede, Netherlands

 (Received 9 June 2020; revised 17 September 2020; accepted 1 October 2020; published 21 October 2020)

Pulsed laser deposition is widely used to synthesize complex oxide thin films with advanced functional properties because of the versatility of the process, although the actual processes and mechanisms that take place are highly dynamic and nontrivial. Detailed understanding of the plume dynamics is required to achieve enhanced control of the growth of complex oxide thin films. However, analytical models of the plasma plume proposed in previous studies, the so-called shockwave model, drag model, and adiabatic thermalization model, only apply to a specific pressure regime and only focus on the propagation of the plasma front. Numerical modeling of the plasma dynamics has previously been pursued for the one-dimensional propagation of a Si plasma plume in a noble background gas. Here we have explored a more generalized numerical model for the dynamics of a TiO₂ plasma plume by extending to three dimensions, multiple elements in the plasma plume, and including chemical reactions in an oxygen environment without the use of adaptive parameters, other than used for the description of the initial plume shape. Comparison between the simulations and the self-emission measurements of the TiO₂ plasma plume shows good agreement. Our model enables detailed simulation of the oxidation state of the arriving particles (Ti, TiO, and TiO₂) on the substrate surface depending on oxygen background pressure. Interestingly, low pressures of about 0.02 mbar result in fast oxygen particles arriving prior to the slower titanium particles, which could significantly influence the oxidation state of the initial substrate surface. The enhanced number of collisions for higher pressures of about 0.1 mbar leads to a large amount of the low-mass oxygen particles coming to a standstill 1–2 cm away from the ablated target. Furthermore, the three-dimensional nature of our model has enabled simulation of the lateral variations in composition of the deposited particles on the substrate surface. Although negligible variations in the Ti:TiO and Ti:TiO₂ ratios are present for high pressures over deposition areas with diameters up to 5 cm, significant variations can be observed for low pressures. These insights could play an important role in upscaling pulsed laser deposition from a scientific laboratory-based scale to an industrial large-area scale.

DOI: [10.1103/PhysRevMaterials.4.103803](https://doi.org/10.1103/PhysRevMaterials.4.103803)

I. INTRODUCTION

Epitaxial engineering has proven to be a successful tool for achieving advanced functional properties in complex oxide thin films, which cannot be obtained in single crystals or polycrystalline samples [1]. Since the successful synthesis of a high-temperature superconducting thin film in 1987 [2], pulsed laser deposition (PLD) has emerged as a versatile technique for the deposition of high-quality (epitaxial) thin films from a wide variety of complex oxide materials, including superconductors, metals, ferroelectrics, ferromagnets, dielectrics, and their multilayers. The PLD technique, used broadly in research laboratories worldwide, is conceived as relatively simple, mainly because of the fact that the heating source for evaporation (ablation), i.e., a powerful laser, is located outside the process chamber. Although PLD derives its popularity from its versatility, the actual processes and mechanisms that take place (during ablation, in the plasma plume, and on the substrate) are highly dynamic and nontrivial.

During the expansion of the plasma plume, there is a strong interaction between the vaporized particles due to the high instantaneous ablation rates. Although the vapor does not gain energy after the laser pulse has ended, these collisions cause an important redistribution of energy among the various degrees of freedom of the thermodynamical system of the superheated plasma plume. The processes in the propagating plume are influenced by the background gas parameters, i.e., mass and pressure, and, as a result, interactions and reactions are taking place which determine the kinetic energy of the particles arriving at the substrate. This kinetic energy can be varied from high energy (~ 100 eV) in vacuum to low energy (~ 1 eV) at ambient pressures and can be used to modify thin-film growth. In recent years, much has been learned about the nature and composition of arriving (reacted) species by means of laser-induced fluorescence detection [3,4] as well as their role in the deposition process on the observed type of thin-film growth [5–7].

A detailed understanding of the plume dynamics is required to achieve enhanced control of the growth of complex oxide thin films. Accurate modeling of the oxidation state, energy, and spatial distribution of the arriving species is crucial for successful prediction of the required deposition

*m.huijben@utwente.nl

parameters to obtain high-quality thin films with specific functional properties. In previous studies three different analytical models have been proposed to describe the plasma plume, the so-called shockwave model [8], drag model [9], and adiabatic thermalization model [10]. In the first model a shockwave is generated by collisions of the front of the plume with the background gas [8]. The initial shockwave in the background is accompanied by an internal shockwave within the plume, changing the internal density of the plume. The general requirement for this model is that the mass of the ablated material is much lower than the mass set in motion in the background gas. For a typical PLD plasma plume this is not the case, especially at low-background-pressure conditions. In the drag model the plasma is assumed to be a solid body, which moves through a gas and experiences viscous friction [9,11]. This assumption is valid in the initial phase of the PLD plasma plume expansion when the plume is extremely dense (often said to be as dense as a solid), but at the later stages of propagation this condition is not fulfilled anymore because of the plume expansion. Furthermore, the drag coefficient of a body depends on its shape and the medium in which it propagates. The PLD plume changes shape during its propagation and therefore the drag coefficient needs to be considered dynamic in nature.

The PLD plasma conditions are on the boundary of the shockwave and drag models. The drag model is more appropriate for low pressures and/or the initial propagation phase, while the shockwave model is more suitable for high pressures and/or the later propagation phase. Both models assume a fluidlike behavior and only focus on the propagation of the plasma front. This is the location where most of the interactions between the plasma and background gas occur and also where the oxidation of the species is expected. However, knowledge about the plasma front does not provide sufficient information about the composition and oxidation to relate the plasma plume dynamics fully to the film growth. Furthermore, both models require several experimental parameters to describe the propagation of the plasma front which are difficult to predict in advance. In the adiabatic thermalization model the front of the plasma plume is described as an ionized plasma layer that expands from the target surface as it is driven by the pressure gradient [10]. It allows the determination of a characteristic distance at which the particles lose their unidirectional velocity, scatter, and thermalize. However, the model determines the range of the plume without considering the angular distribution, composition, or oxidation of the plasma plume. Therefore these models cannot accurately predict the propagation of the plasma plume when variations to the PLD parameters are made: for example, by using different target materials, background gas pressures, laser fluences, etc.

Numerical modeling of the plasma dynamics is challenging due to the large number of particles (10^{15}) in the PLD plume. This multiscattering approach has previously been pursued by Wood *et al.* for the one-dimensional propagation of a Si plasma plume in a noble background gas [12,13]. However, the possible presence of multiple elements in the plasma plume was not included in the model, as well as the possible oxidation of the species in the plasma plume during propagation towards the surface of the grown thin film. Here we will explore a more generalized numerical model for the plasma

plume dynamics of complex oxide materials by extending the Wood's model to three dimensions, allowing for multiple elements in the plasma plume and including chemical reactions in an oxygen environment without the use of adaptive parameters (apart from two parameters that define the initial plume shape, to be discussed later, and that are determined experimentally from this shape). The model tracks the composition and velocity distribution of the (reacted) species in finite volume elements of the plume over time. Our model enables detailed simulation of the oxidation state of the arriving particles (Ti, TiO, and TiO₂) on the substrate surface, depending on the oxygen background pressure. Furthermore, the three-dimensional (3D) nature of our model enables simulation of the lateral variations in composition of the deposited particles on the substrate surface. The processes taking place on the substrate surface after arrival are not a topic of this study.

II. NUMERICAL MODEL

A. Initial ablation

The interaction of the laser beam with the target material is affected by a number of parameters, such as the absorption coefficient and reflectivity of the target material, as well as the pulse duration, wavelength, and energy of the laser beam. In general, the interaction between the laser radiation and the solid material takes place through the absorption of photons by electrons of the atomic system. The absorbed energy causes electrons to be excited to higher energy states in the atom; the atom can even become ionized, and as a result, the material heats up to very high temperatures in a very short time. Due to the high temperature and the high excitation state of the atom, some material will be evaporated and will cause additional absorption of energy, causing additional excitation of the electrons in the evaporated atoms. The temperature of the evaporated material therefore rapidly increases to extremely high values. This effect leads to a very high pressure near the target, and due to the pressure gradient with the low-pressure background gas the plume of evaporated material will expand. The ablated particles will move predominantly in the direction perpendicular to the target surface. Because of deexcitation and rapid cooldown of the atoms in the expanding plasma, these excited particles will emit photons, also in the visible range, which is characteristic for the laser ablation process.

Particle-by-particle modeling of a plasma plume, consisting of in the order of 10^{15} particles, in which each particle has a different velocity and oxidation state, is beyond common simulation capabilities. However, for the growth of a film the distribution of the characteristics of the arriving species is important. Ordering the particles in a number of groups with similar properties will greatly reduce the computations and will enable detailed modeling of plasma plume parameters influencing the film growth. Therefore a model was developed that allows the detailed determination of the temporal development of the composition, density, and velocity v distribution and oxidation state of the atoms in a specific volume element ΔV , depending on its radial r and angular θ location (see Fig. 1). This enables the characterization of the type and energy of the ablated species after a specific time and the

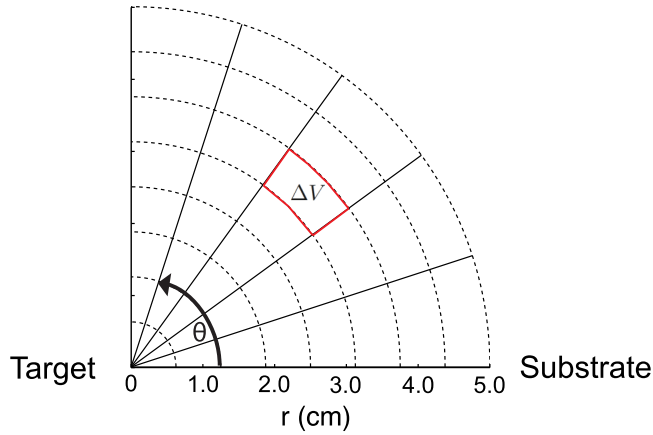


FIG. 1. Polar grid for the numerical model with $r = 0$ and 0.05 m for the positions of target and substrate, respectively.

number of collisions on the route from target to substrate. The plume conditions can be varied in order to change the oxidation state of the particles arriving at the substrate.

For the deposition of an oxide thin film, the simplest form of an oxide target would be a MO_x target, consisting of a metallic ion M and an oxygen ion O . Calculating the initial velocity of the plume can be done by setting up an energy balance equation for the ablation per laser pulse, which has the form

$$E_{\text{laser}} = A \left[N_{uc} \left(E_b + \sum_{i=1}^m [E_k(i) + \Delta E_{\text{exc}}(i)] \right) + Q \right] \quad (1)$$

Here E_{laser} is the energy of a single laser pulse. Depending on the material and the target surface structure, a fraction of this light will be absorbed or reflected when hitting the target: A (with a value in the range $0 \dots 1$) represents the fraction of absorbed energy, and N_{uc} is the total number of ablated unit cells. This can be calculated from the ablated volume per laser pulse, the volume of the unit cell, and the target density. E_b is the binding energy per unit cell, required to break up the unit cell and free the atoms to vacuum. As discussed above, there may be multiple elements in one unit cell, and for each element i with mass m_i , energy is transferred. This will go partially into a kinetic energy part $E_k(i) = \frac{1}{2} m_i v_i^2$ and to the excitation of the electrons to higher energy levels ΔE_{exc} . In addition, this term may also contain rotational energy of the emitted atoms. Energy is also transferred as heat loss Q into the target. Typically, for ceramic targets the heat loss is low, as can be inferred from the common experimental observation that the ceramic target does not heat up much, even after prolonged ablation; therefore this will be neglected in this model. Due to the duration of a KrF laser pulse (~ 20 ns), the first ablated particles already start to move away from the target, while the pulse is still active. These initially ablated atoms absorb some additional energy from the laser pulse, which boosts the atoms in a higher excited state.

In the first (tenths of) microseconds after the impact of the laser pulse with the target the dominant velocity component of the ablated particles is in the radial direction causing the plume expansion. In this phase the atoms do not collide yet with the surrounding gas molecules/atoms, and thus no

energy transfer to the background gas has taken place. The loss of energy by light emission is a loss from the internal energy of the atoms in the plasma. We expect that this loss is not (partly) supplemented by kinetic energy due to atomic collisions in the plasma, because the atoms in the plume all move approximately in the same (forward) direction and atoms of different type rapidly separate in space due to their different velocities and therefore also cannot interact with each other. In combination with the limited lifetime of the excited states, this would also explain the rapid decrease of the intensity of the expanding plasma. This in turn means that the atoms cannot obtain a nonradial velocity component; thus in the initial plume all particles predominantly have a radial nonzero velocity component, which is then the only degree of freedom. This implies that the velocity of the oxygen atom is significantly higher than that of the metal atom by a factor of 1.7 in the case of a Ti oxide target due to the nearly a factor of 3 difference in atomic mass.

Mao *et al.* investigated the initial ablation [14], and in their model a homogeneous ablation of individual atoms was assumed. No big clusters or groups of bonded particles are ablated from the PLD target, and initially the individual ablated atoms have no bonds with other atoms. After the initial ablation the plasma becomes approximately spherical about 100 ns after the laser pulse hits the target (as was determined from experimental observations) and propagates through the background gas. The starting point of our model is therefore set at $t_0 = 100$ ns, and the initial ablation is outside the scope of our model. The large radial velocities and the spherical expansion of the plasma plume front found in the initial phase of the plasma support the assumption that the tangential velocity of the particles in the initial plume are (negligibly) small as compared to the radial velocity. Further, we assume that the angular particle velocity distribution takes the following shape, usually adopted for particles leaving a target after impact by a high energetic particle:

$$f(\theta) = \frac{1}{N_{\text{tot}}} \frac{dN_{\text{ini}}}{d\theta} = \frac{\cos^n \theta}{N_{\theta}}. \quad (2)$$

Here $dN_{\text{ini}}/d\theta$ is the fraction of the initial number of particles per unit angle, N_{tot} is the total number of ablated particles, N_{θ} is a normalization factor given by $N_{\theta} = \int_0^{\frac{\pi}{2}} \cos^n(\theta) d\theta$, and the positive, real parameter n is the coefficient that determines the shape of the initial plasma plume and is used here as a fitting parameter of the initial angular distribution. We expect that its value depends on the pulse energy, with larger n corresponding to a more forward-oriented plume arising at high E_{laser} . This pulse energy dependence is not explored further here. For each angle there is a particle velocity distribution for the particles in the plasma. We assume for simplicity that the initial radial, particle velocity distribution of particle type i is the same for all angles θ and is given by a Gaussian distribution function,

$$f_i(v) = \frac{1}{N_{\text{tot}}} \frac{dN_{\text{ini}}}{dv} = \frac{1}{\sigma_v \sqrt{2\pi}} \exp\left(-\frac{(v - v_c)^2}{2\sigma_v^2}\right), \quad (3)$$

where v_c is the center velocity of the distribution and determined by the average kinetic energy of the particles $E_k(i) = \frac{1}{2} m_i v_i^2$, obtained from fitting to the experimentally determined

initial expansion velocity of the plume, and σ_{v_i} is the standard deviation. The description of the plume expansion is not very sensitive to the actual shape of the velocity distribution, as long as it peaks at a given value and falls off with a certain width. We have chosen this one-dimensional Gaussian distribution, since we have no indications that the distribution is very asymmetric. Note that a one-dimensional Maxwell-Boltzmann distribution superimposed on an average radial velocity would allow one to relate the width of the distribution with a particle temperature based on the kinetic energy distribution, $\sqrt{kT_{pl}} = \sigma_v$. The value of σ_{v_i} is chosen on the basis of experimental fitting. Formally, $f_i(v)$ is cut off at $v = 0$, so that in the initial plasma there are no particles moving towards the target. However, since the average velocity is very high and σ_{v_i} relatively low, there are no particles to be taken into account with negative radial velocity. In the course of time, due to collisions with the background gas, particles can obtain also a negative velocity, which is taken into account in the model.

Figure 2 shows the initial particle velocity distribution of a TiO_2 plasma plume for any angle θ . For a spherical coordinate system with coordinates (θ, ϕ, r) , the particles can be grouped into velocity bins Δv , within an angular bin $\Delta\theta_j$ around θ_j , with j the number of steps to cover the angular range between 0° and 90° with starting time $t_0 = 0$ and initial position $r_0 = 0$. This transforms Eqs. (2) and (3) into

$$\Delta V(r_0, \theta_j) \Delta v = \int_0^{2\pi} d\phi \int_{\theta_j}^{\theta_j + \Delta\theta} \sin(\theta) d\theta \int_{v_k}^{v_k + \Delta v} dv, \quad (4)$$

$$\begin{aligned} \Delta N_{\text{ini}}(\theta_j, v_k, t_0, r_0) &= N_{\text{tot}} f(v) f(\theta) \Delta V(r_0, \theta_j) \Delta v \\ &= N_{\text{tot}} \left[\frac{\cos^n \theta_j}{N_\theta} \right] \left[\frac{1}{\sigma_v \sqrt{2\pi}} \exp\left(-\frac{(v_k - v_c)^2}{2\sigma_v^2}\right) \Delta v \right] \\ &\quad \times [(\cos(\theta_j + \Delta\theta) - \cos \theta_j)] 2\pi. \end{aligned} \quad (5)$$

For complex oxide materials, a PLD target consists of more than a single element, and each element will have its own initial particle velocity distribution. When a single element plasma plume propagates through a vacuum, thus without collisions, the velocity distribution of the particles within the plume would remain the same, and the plasma density decreases over time because the plume expands due to the angular distribution of the velocity vectors. However, if the plasma consists of multiple elements, for example, Ti and O, as in Fig. 1, one expects that the fast Ti atoms catch up with the slowest O atoms, and collisions (and even chemical reactions) may occur in the range where the velocity distributions overlap, causing a change of the velocity distributions because momentum is transferred from the heavy atom to the light atom in the case of elastic collisions. When the plume expands in a background gas there will be additional interaction with the background gas atoms or molecules.

B. Collisions and interactions

When the ablated particles are traveling through the background gas from the target towards the substrate surface, they will undergo numerous collisions and interactions depending

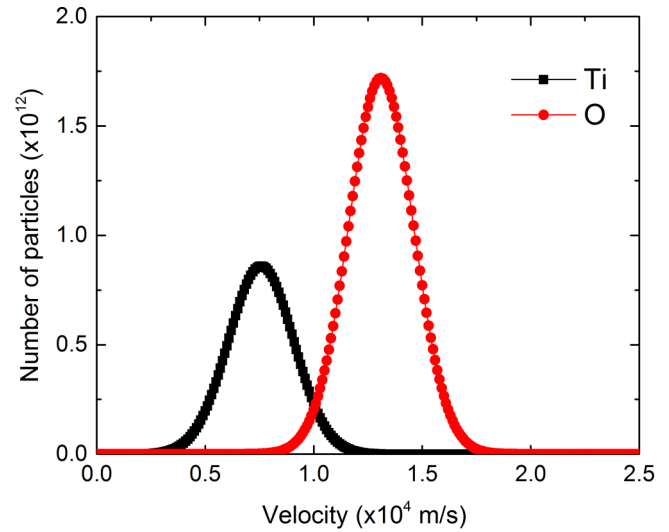


FIG. 2. The distributions of the initial velocities for the titanium and oxygen particles within the TiO_2 plasma plume, assumed to be Gaussian distributed. The medians of the distributions were estimated using Eq. (1), while the distribution width is determined from the measured velocities of the center and the front of the visible Ti plasma plumes and is assumed to be equal for Ti and O.

on the deposition parameters. To describe the collisions in the plasma, we use a simple description, namely, elastic (or fully inelastic in the case of an interaction) collision between point masses in one dimension. A second consequence of considering only pointlike particle collisions is that in the collisions no kinetic energy can be transferred to rotational energy states of the atoms and multiatom particles (or vice versa). In principle, such a process would further slow down the plasma, especially in the later stages when the cumulative number of collisions has become large. We note that such a mechanism might be an explanation for the observed differences between experimental plasma front positions and the modeled curves in Figs. 4 and 6. This is a significant simplification of the real situation, in which finite-sized particles can scatter in different angles when they do not collide head-on, requiring considerably more computational effort. Assuming one-dimensional, and hence head-on collisions, means that the particles move, and keep moving after the collision, along the same (radial) line and that there is no energy, momentum, and particle exchange between different angular bins. Rigorous proof of the validity of these simplifications is beyond the scope of this paper. We see in the fact that the model gives a reasonably good description of the plasma expansion process an experimental justification of the simplifications made. Equations (6) and (7) provide the new velocities of the particles after a head-on collision, which are dependent of the mass and velocity of both particles. Furthermore, we assume that $v_2 = 0$, which is the (average) velocity of the relatively cold background gas:

$$v'_1 = \frac{v_1(m_1 - m_2) + 2m_2v_2}{m_1 + m_2} \approx \frac{v_1(m_1 - m_2)}{m_1 + m_2}, \quad (6)$$

$$v'_2 = \frac{v_2(m_2 - m_1) + 2m_1v_1}{m_1 + m_2} \approx \frac{2m_1v_1}{m_1 + m_2}. \quad (7)$$

A positive sign of the velocity means forward-directed velocity. Note that when a metal plume atom is heavier than the background gas (usually O_2 with $M = 32$ u or Ar with $M = 40$ u), which is mostly the case, then part of the kinetic energy is transferred to the background gas, which gains forward velocity and the plume atom is slowed down. However, for lighter elements such as Li, Na, and even Al, the metal atom can be reflected backwards. The latter may account, for example, for the difficulty in transferring them from a stoichiometric target to the substrate in the same ratio. It is possible to make an estimate of the velocities in the background gas by calculating the average kinetic energy of the background gas:

$$E_{k,avg}^{bg} = \left[\frac{1}{2} m_{bg} v_{bg}^2 \right] = \frac{3}{2} k_b T_{bg}, \quad (8)$$

where m_{bg} is the mass of the background atom or molecule with its average velocity v_{bg} at a given background gas temperature T_{bg} . For a temperature of 20 °C the mean velocity is around 400 m/s. The Ti atoms in the plume have initial velocities of the order of 1×10^4 m/s. This difference in velocity is so large that the velocity of the background becomes insignificant. Only at high deposition pressures and at the later stages of the plume propagation, the velocities of the particles in the plume become of the order of the background gas velocity. There is no preferential direction of the gas particles in the background. That would mean that in the event of a collision the velocity of the background gas particle could be in any direction with respect to the direction of motion of the plume particle. The average background gas velocity, with which a plume particle would collide, is therefore equal to zero, which we will assume in the calculation when modeling the collisions with the background gas. In principle one can take account of the effect of a heated substrate, that locally changes the gas density, by calculating the static temperature profile through the background gas. This refinement was not applied in this study. The starting background gas density is simply given by the background pressure and temperature as $\rho_{bg}(t_0) = p_{bg}/kT_{bg}$.

As already mentioned above, due to the high velocity and generally higher mass of the plasma atoms the background particles on average obtain a higher velocity after a collision. As an example, a Ti atom is considered with an initial velocity of 1×10^4 m/s that collides with a zero-velocity oxygen molecule in the background gas. Following Eq. (7), the oxygen particle obtains a velocity of 9×10^3 afterwards. The initial front velocity of Ti atoms in a plasma ablated from a TiO_2 target is on the order of 1.3×10^4 m/s, and the final velocity of the plasma front atoms after the collision is about 1×10^3 m/s for 0.1-mbar background pressure. This leads to a kinetic energy difference of 42 eV per Ti particle. Using the equations above a decrease of this magnitude would require about two to three collisions. From calculations assuming only inelastic collisions (i.e., chemical reaction to TiO and TiO_2) it is concluded that reacted particles do not slow down very much, in contrast to elastic collisions. Thus, while the majority of Ti atoms that experience elastic collisions are rapidly slowed down, the particles that react in a first, inelastic collision would move in front and away from the slowed-down Ti plume. From the experiments discussed further on it is seen

that this is not observed experimentally, as it would show up in a plume separating in a slowing-down Ti plume with a Ti oxide plume in front. In contrast, inelastic collisions, i.e., the creation of Ti oxide particles, only occurs after slowdown of the Ti particles by elastic collisions, so that the front of the slowing-down Ti plume starts to react to Ti oxides. This implies that inelastic collisions only can happen at low particle velocities. This, in turn, explains why in a low-density background, in which there are only few collisions that slow down the Ti atoms, one observes very little Ti oxide formation.

Several types of interactions are possible within the plasma plume and between the plasma plume and the background gas. Starting from a M_xO_y target, the M and O atoms can both elastically collide with the background gas particles with a random velocity and direction. These collisions push the background forwards, generating a pressure wave inside the background. In order to describe the propagation of the plume, the density of the background and that of the plume must be calculated. This results in the following seven possibilities: (1) a metal particle M with a stationary background particle (e.g., oxygen atom O_{bg}), slowing the metal particle down as well as increasing the energy of the background particle and propagating it forwards ($M-O_{bg}$), and (2) a metal particle can elastically collide with a high energy propagating background particle. (3, 4) These two cases also hold for interactions between the ablated oxygen particles and the background particles ($O-O_{bg}$). Furthermore, the following interactions within the plasma plume could be possible: (5) $M-M$, (6) $O-O$, and (7) $M-O$. When an $M-O$ interaction occurs, the formation of the reaction product MO could occur, generating more particle types and thus more types of interactions. More complex targets with more elements would dramatically increase the number of possible interactions, thereby increasing the calculation time for the numerical modeling. For example, a $M_xM_zO_y$ material compound would result in 12 possible interactions.

By calculating the distributions, instead of following the individual particles, the $M-M$ or $O-O$ interactions are relatively rare since these atoms will separate in space because of their difference in velocity. When two similar atoms, $M_1(r_i, \theta_j, v_{k_1}, c_o) \approx M_2(r_i, \theta_j, v_{k_2}, c_o)$, with different velocities but moving in the same direction, have an elastic collision, the velocities of the two plasma particles would interchange. This results in no net change of the plasma velocity distribution, thus no change in the plasma dynamics. Such collisions would cause a change in the velocity distribution only if inelastic collisions would occur, forming a metallic cluster or an O_2 molecule, which we exclude since we have no indications from the experimental observations that this occurs on a significant scale. Therefore $M-M$ and $O-O$ interactions are not taken into account in our model.

In the first stage of the propagation of the plasma significant self-emission of the metal particles can be observed (as will be discussed more extensively in a later section), as the plasma plume exhibits the highest plume temperature in the initial stages after ablation. If the self-emission would be due to a significant number of $M-M$ interactions, also a decrease in the plume velocity should be expected because of a loss of kinetic energy, which is not the case as a constant velocity is observed. In the next stage of plume propagation, in

which the plume front velocity is decreasing, also significant self-emission of the metal atoms is observed. However, the density of the plasma plume also decreases significantly so that excitations due to M - M interactions are even less likely. Therefore M - M interactions are not assumed to be an important contributor to the processes taking place in the plasma plume.

The number of M - O_{bg} interactions depends on the particle density of the background gas. Fast plume particles interact with the background, scattering background gas particles to other positions and changing the local density, in turn changing the interaction probability for slower particles. This implies that not only the plasma plume must be simulated but also the motion of background gas particles, and the change in density of the background gas should be taken into account. Typically the velocities of the scattered particles in the background gas are high, and as a result the collisions push the background gas forwards in front of the PLD plume.

When the initial particle distribution collides with the background gas the velocity distribution changes. The collision probability in a time step Δt is determined by the local mean free path of a single particle due to the local background density and can be expressed as

$$R_{1,p-bg}(v_k, u_m, t_{n+1}) = \rho_{bg}(r_i, \theta_j, u_m, t_n) \sigma_{bg} v_k \Delta t. \quad (9)$$

The collision probability $R_{1,p-bg}$ for a single particle between the plasma atom with velocity v_k and the background particle with velocity u_m in the time interval Δt is determined by the local background particle density and the distance traveled by the ablated particle. ρ_{bg} is the local background density of particles with velocity u_m at position r_i, θ_j at time step t_n , and σ_{bg} the cross section for the collision of the plume particle with the background gas particle, defined as the sum of the kinetic cross sections of two colliding hard sphere particles. The number of particles $\Delta \Delta N_{p-bg}$ in a given volume element $\Delta V(r_i, \theta_j)$ that collide with the background gas is proportional to the number of particles $\Delta N(r_i, \theta_j, v_k, t_n) = f(r_i, \theta_j, v_k, t_n) \Delta V(r_i, \theta_j)$. The collided particles have changed position $r'_i = r_i + dr$, velocity $v'_k = v_k + dv$ with $dr = v'_k \Delta t$. We also keep track of the number of collisions, $c'_p = c_p + 1$, the particles in a given bin have on average. Hence the scattered particles can move to a different volume element and be counted in a different velocity and collision number bin:

$$\begin{aligned} \Delta \Delta N_{p-bg}(r_i + dr_i, \theta_j, v_k + dv_k, u_m, t_{n+1}, c_p + 1) \\ = \rho_{bg}(r_i, \theta_j, u_m, t_n) \sigma_{bg} v_k \Delta t \Delta N(r_i, \theta_j, v_k, t_n, c_p). \end{aligned} \quad (10)$$

The total fraction F_s of the plume particles in bin ΔV that has been scattered in the time step $t_n \rightarrow t_{n+1}$ is

$$F_s(r_i, \theta_j, v_k, t_{n+1}) = \frac{\sum_{c'_p} \Delta \Delta N_{p-\rho_{bg}}(r'_i, \theta'_j, v'_k, t_{n+1}, c'_p)}{\sum_{c_p} \Delta N(r_i, \theta_j, v_k, t_n, c_p)}. \quad (11)$$

The not-scattered fraction F_{ns} of plume particles is

$$F_{ns}(r_i, \theta_j, v_k, t_{n+1}) = 1 - F_{sc}(r_i, \theta_j, v_k, t_{n+1}). \quad (12)$$

By summation over all the fractions scattered in different volume elements at background gas particles with different velocities to the volume element at (r'_i, θ'_j) one obtains the

velocity distribution of the influx of scattered particles in that element:

$$\begin{aligned} \Delta \Delta N_{p-bg}(r'_i, \theta'_j, v'_k, t_{n+1}, c'_p) \\ = \sum_{r_i, v_k, u_m, c_p} \Delta \Delta N_{p-bg}(r_i \rightarrow r'_i, \theta_j, v_k \rightarrow v'_k, u_m, t_{n+1}, c_p). \end{aligned} \quad (13)$$

This provides the velocity and position distributions for each new time step. The plasma plume particle distribution in the next time step for ΔN_p becomes the sum of the nonscattered plasma particles $\Delta \Delta N_{ns}$ and the particles that collide with the background gas $\Delta \Delta N_{p-bg}$:

$$\begin{aligned} \Delta N_p(r_i, \theta_j, v_k, t_{n+1}, c) \\ = \Delta \Delta N_{ns}(r_i, \theta_j, v_k, t_{n+1}, c) \\ + \Delta \Delta N_{p-bg}(r_i, \theta_j, v_k, t_{n+1}, c). \end{aligned} \quad (14)$$

A similar calculation is performed for the background gas particles simultaneously, so that at any time step also the background gas density can be calculated, accounting for the interaction with the plume. To summarize the procedure: Due to the assumption that the exchange of particles between different angular bins can be neglected, one can describe the 3D expansion of the plume by the propagation of the plume for each angular bin separately, in which particles interact predominantly by forward and backward scattering from each other along a radial direction in a one-dimensional (1D) description. The good correspondence of the numerical results with the experimental observations of the plasma plume propagation and expansion and the internal chemical interactions justifies this important simplification and keeps the computational cost at a manageable level.

III. EXPERIMENTAL AND NUMERICAL RESULTS

A. Experimental details

To evaluate our model, the PLD plasma plume of the well-known compound TiO_2 was investigated and compared to experimental results. It has been shown in previous studies that with varying PLD deposition conditions different TiO_2 crystal structures, e.g., anatase and rutile, can be created [15,16]. A higher substrate temperature and/or lower oxygen background pressure in general produces a rutile phase, while a lower temperature and/or higher oxygen pressure creates the anatase phase. We will study the influence of the oxygen background pressure on the propagation and oxidation of the plasma plume, created by ablation from a TiO_2 target.

Optical emission spectroscopy (OES) is used to study the spectral composition of the plasma plume to observe the specific elements and to determine their oxidation state. A high-temperature plasma emits light, as highly excited ions make a transition to a lower energy state and emit photons. Analysis of the wavelengths of the emitted photons should, in principle, make it possible to observe the oxidation state of the different elements of the plume. However, the drawback of these self-emission measurements is the fact that only the particles which emit light are visible. Particles with a low energy, created during the initial ablation or due to collisions,

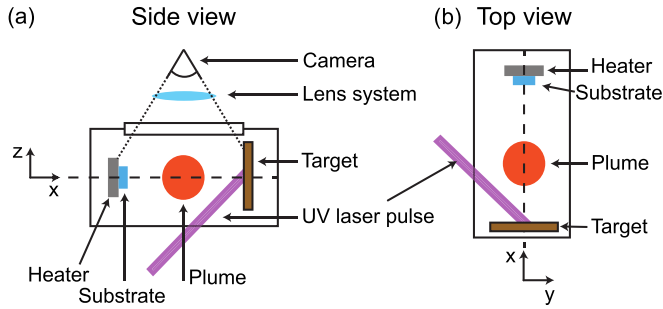


FIG. 3. Schematic side (a) and top (b) view of the PLD system with the OES camera setup.

are not measurable. Therefore self-emission measurements are only able to analyze the relative changes within the plasma plume, but conversion of the measured light intensity at a given wavelength to an absolute number of particles is not possible.

In order to obtain self-emission measurements of the spatial and temporal propagation of the plume during the ablation, a fast-response optical camera was installed onto the PLD setup perpendicular to the plasma plume, see Fig. 3. The camera is sensitive for wavelengths in the range of 300–800 nm. The experimental images, as shown in Figs. 4 and 6, are a combination of the intensity profiles along the plume heart line (x direction in Fig. 3) in the x - y plane and integration of the intensity in the perpendicular orientation (z direction). The position along the x axis is predominantly determined by the average velocity distribution (as long as no collisions have taken place) of the particles at that position up to the time t of the measurement, whereas the y position [$y = x \cdot \tan(\theta)$] mainly is determined by the angular distribution of the plasma. The measurements and simulations are done for PLD conditions at room temperature in a low and a high oxygen pressure of respectively 0.02 and 0.1 mbar. The plume was ablated from a single-crystal anatase TiO_2 target with a laser

energy density of 2.0 J/cm^2 , a spot size of 2.1 mm^2 , and a target-substrate distance of 5.0 cm . Figure 4 displays the self-emission of the PLD plume at different time intervals after the laser pulse for a background oxygen pressure of 0.02 mbar. The bottom red line is the location of the target, and the top blue line is the location of the substrate on the heater. The exposure time and gain settings of the camera were adjusted for the images at the different time intervals. The values for the applied exposure time and gain are included in Fig. S1 in the Supplemental Material [17], together with a color bar for the used intensity scale in all images. It can be concluded that the intensity after $7 \mu\text{s}$ is about a factor of 6000 lower than the intensity after $1 \mu\text{s}$ for plasma propagation at a low pressure of 0.02 mbar.

The initial PLD plume at such low pressure has a nearly spherical shape. The typical temperature of the plasma directly after ablation is about $\sim 1 \times 10^4 \text{ K}$ [18], Therefore velocities immediately after ablation can be as high as $2 \times 10^4 \text{ m/s}$ [19]. The initial velocity distributions for the titanium and oxygen particles at $t = t_0 = 0$ were calculated by using Eq. (1), assuming no energy loss Q and no pulse energy being converted to excitation energy. As the anatase TiO_2 crystal structure exhibits a tetragonal unit cell with lattice parameters of $a = 3.78 \text{ \AA}$ and $c = 9.51 \text{ \AA}$, the ablated volume is calculated as 1.1×10^{15} titanium atoms and 2.2×10^{15} oxygen atoms per laser pulse for an ablation depth per pulse of $\sim 100 \text{ nm}$. The bond dissociation energy for TiO_2 is $\sim 3.25 \text{ eV}$ [20], and the absorption coefficient of TiO_2 at 248 nm is set at 0.66 [21]. Assuming no energy loss Q and no pulse energy being converted to excitation energy, the velocity of the particles can be calculated using Eq. (1). A velocity of $0.76 \times 10^4 \text{ m/s}$ is obtained for the titanium atoms and $1.32 \times 10^4 \text{ m/s}$ for the oxygen atoms (in accordance with Fig. 2 and $m_{\text{Ti}}v_{\text{Ti}}^2 = m_{\text{O}}v_{\text{O}}^2$). Note that the fast oxygen atoms are not visible with the camera used since the emission lines are outside the spectral window. Thus the observed plume in Fig. 4 is that of the emission lines of Ti. The width of the velocity σ_v distribution is set at $0.15 \times 10^4 \text{ m/s}$, which is estimated using the

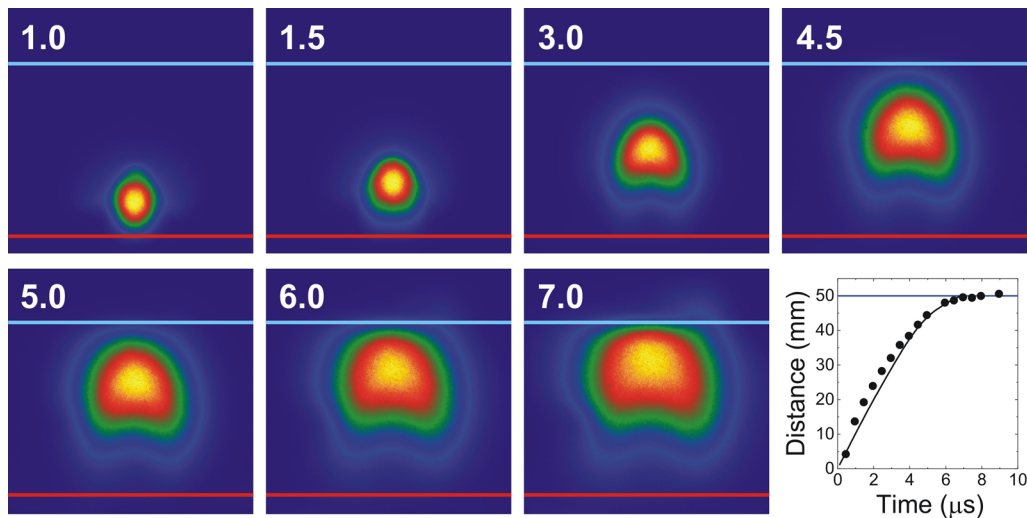


FIG. 4. Self-emission measurements of a PLD plume after different time intervals (in μs), ablated from a TiO_2 target at an oxygen pressure of 0.02 mbar. Locations of substrate and target are indicated by blue and red lines. Experimental (circles) and simulated (line) propagation of the plasma front.

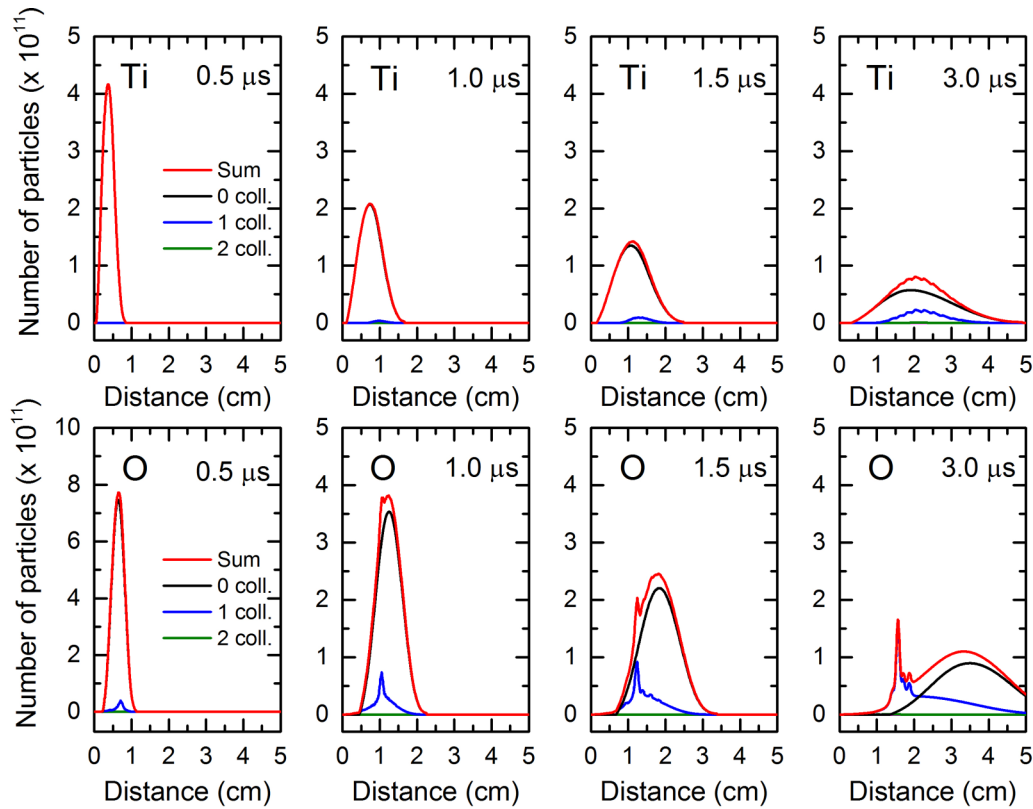


FIG. 5. One-dimensional simulation of the distribution of the Ti and O particles within the TiO_2 plasma plume at an oxygen background pressure of 0.02 mbar at different times and the specific number of collisions. The colors black, blue, and green represent the number of particles that collided zero, one, or two times, respectively. The red line is the sum of all the particles.

measured velocities from the center and front of the initial plume.

Using the calculated average velocities and the fitted σ_v values, the initial velocity distributions as shown in Fig. 2 were calculated. From the angular width of the initial plume at a given intensity percentage of the maximum intensity one can estimate the power n of the angular distribution given by Eq. (2). In this study no effort was made to relate the power n to the ablation conditions, but comparing the values obtained for 0.02 and 0.1 mbar background pressures and otherwise the same ablation conditions, there appears to be a decreasing trend of n with increasing pressure. We note that for any value $n > 1$ the angular distribution has a near Gaussian profile with decreasing width for higher n and hence a more forward-oriented plume.

Figure 4 shows that at low pressure the plume expands during propagation; however, the shape of the front of the plume remains spherical until just before arriving at the substrate. In theory there could always be a few particles that propagate towards the substrate at a high velocity without colliding with the background gas, but the number of these high-velocity particles is low and in general below the detection limit of the OES camera. A generally used parameter to characterize the plasma plume is the position of the front of the plume as a function of time. We will do that here, as well make a connection with the earlier, simpler plasma models. Because of the distribution of velocities, the usual position is taken at a specific percentage of the maximum observed intensity of the plume along the x axis at that time. From the above discussion

it is already clear that the fast part of the plume is moving ahead of this position and that even for other not-visible plume components (here the oxygen component) the front can be moving much faster (here about 2.5 times as fast).

B. 1D and 3D models for plasma propagation

For the investigation of the plasma plume propagation in such low oxygen pressures, a simplified one-dimensional model was initially used. Since in the above-described 3D model we have argued that in good approximation there is no net transfer of particles from bins at one angle to bins at a different angle, the results of the 1D model are the same as those obtained from the 3D model for a specific angle, which was taken to be that of the heart line of the plume. The distributions of the titanium particles and oxygen particles are shown in Fig. 5 at different times. Also shown are the distributions for particles that underwent a certain number of collisions. Particles undergoing more than two collisions are not shown, as their contributions are negligible. With this method it is possible to track the propagation of different elements within the plume. At this low pressure the probability for a collision with the background gas is very small, and therefore oxidation of the elements by inelastic collisions was not included. From the figures it is seen that in the first $1 \mu\text{s}$ after ablation almost no Ti particles collide, while at later times more Ti particles collide and some even come to a standstill between the target and substrate. Due to the higher initial velocity of the O particles as compared to the

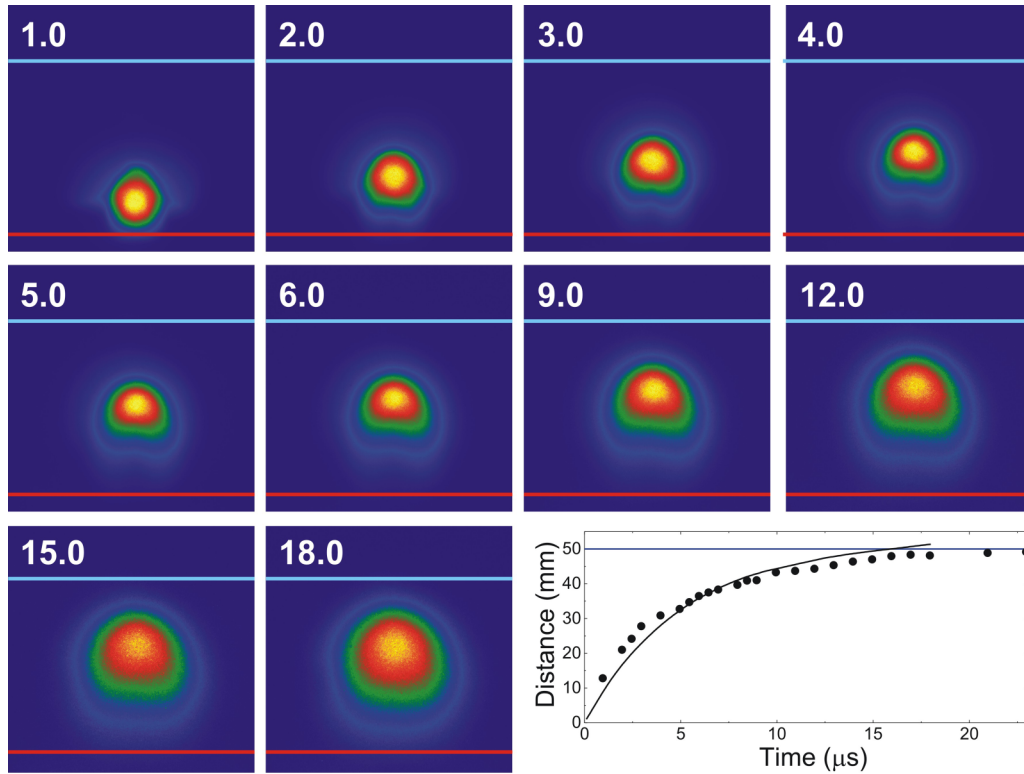


FIG. 6. Self-emission measurements of a PLD plume after different time intervals (in μs), ablated from a TiO_2 target at an oxygen pressure of 0.1 mbar. Locations of substrate and target are indicated by blue and red lines. Experimental (circles) and simulated (line) propagation of the plasma front.

titanium particles, the oxygen part of the plume travels in front of the titanium part and undergoes collisions with the background gas earlier. More O particles come to a standstill as compared to the Ti particles because of the lower mass of the O particles and thus a relatively higher velocity being transferred to the oxygen molecules in the background. This can be observed in Fig. 5 in the peak formation about 1.5 cm away from the target. However, due to the low background pressure of 0.02 mbar the number of collisions is still limited, and therefore the change in the average velocity of the Ti and O particles in this one-dimensional simulation is very small. This can also be observed in the location of the simulated front of the plume at different time intervals after ablation, see Fig. 4. The simulated propagation behavior of the plasma front is in good agreement with the experimental results obtained from OES analysis of an ablated TiO_2 plasma plume.

When the oxygen background pressure is increased from 0.02 to 0.1 mbar, the propagation behavior of the plasma changes due to the enhanced number of collisions, see Fig. 6. The exposure time and gain settings of the camera were adjusted for the images at the different time intervals. The values for the applied exposure time and gain are included in Fig. S2 in the Supplemental Material [17], together with color bars for the used intensity scales in all images. It can be concluded that the intensity after 1 μs in a high pressure (Fig. S2) is about a factor of 1100 lower than after 1 μs in a low pressure (Fig. S1). Furthermore, at these high pressures the intensity after 18 μs is only a factor of 7 lower than the initial intensity after 1 μs . Interestingly, it can be observed that the intensity of the excited particles in the plasma plume arriving at the

substrate surface in a high background pressure (image after 18 μs in Fig. S2) is of the same order of magnitude as when the plasma plume arrives at the substrate surface in a low background pressure (image after 7 μs in Fig. S1).

From the measured propagation behavior in Fig. 6 it can be seen that after about 5 μs the majority of the Ti atoms have collided at least once so that the plume slows down and the plume shape starts to change. The simulated distribution of the titanium particles and oxygen particles confirms this significant increase in number of collisions, see Fig. 7. The Ti particles experience several collisions, which reduces the kinetic energy dramatically and causes the titanium part of the plume to spread out. Although the O particles exhibit a higher initial velocity after ablation, their relatively low mass causes a larger velocity decrease after each collision. Therefore the oxygen part of the plume undergoes an even larger drop in kinetic energy, which causes a substantial part of the O particles to come practically to a standstill after 5 μs . These results show that in general by choosing the substrate-target distance for a given background gas pressure, type of background gas, laser pulse energy, and target materials one can select to a certain extent which and in what ratio particles from the target arrive at the substrate. Note that this selection is a consequence of the spatial separation and halting of plasma particles, which are based on the mass difference of the target elements.

As the real PLD plasma plume propagates in three dimensions, the model is expanded from 1D to 3D, shown in Fig. 8. The results of the simulations are shown at 3 μs after ablation from the TiO_2 target. The images display half of the plasma

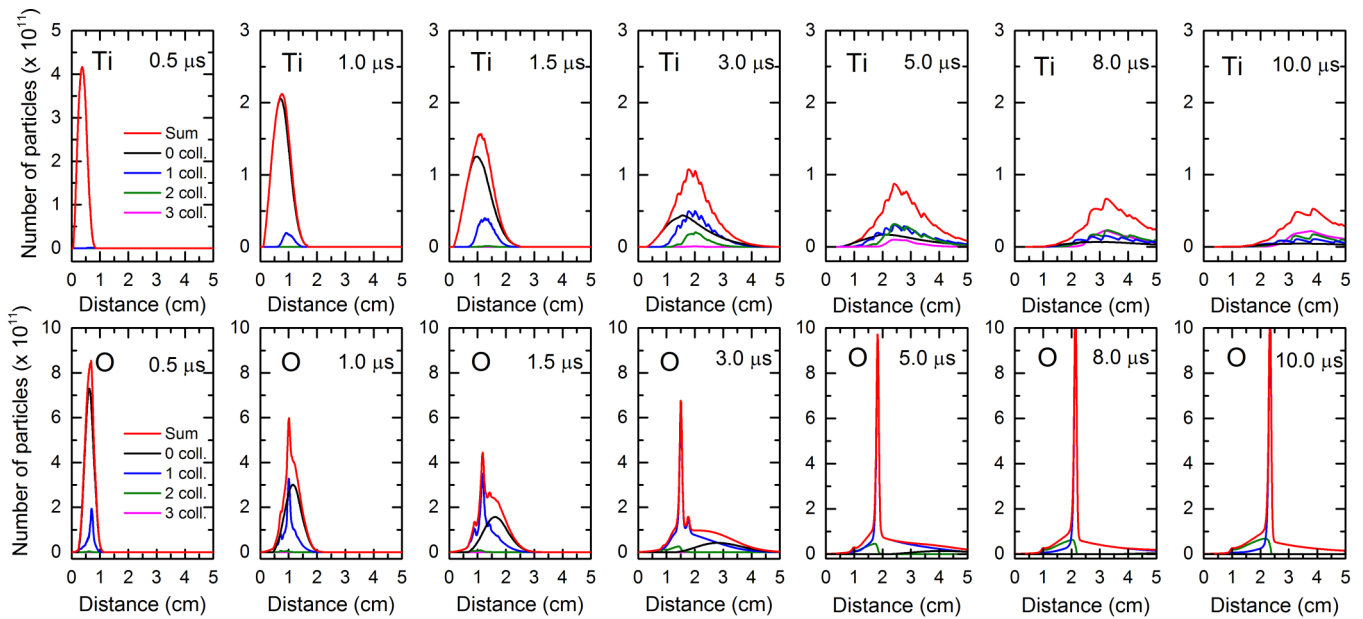


FIG. 7. One-dimensional simulation of the distribution of the Ti and O particles within the TiO_2 plasma plume at an oxygen background pressure of 0.1 mbar at different times and the specific number of collisions. The colors black, blue, and green represent the number of particles that collided zero, one, or two times, respectively. The red line is the sum of all the particles.

in the x - y plane, which can be mirrored in the x axis. The simulations of the propagation of O and Ti particles within the plasma plume have been performed for oxygen pressures of 0.02 and 0.1 mbar.

The titanium part of the plasma plume expands in all directions while propagating forward towards the substrate at an oxygen background pressure of 0.02 mbar. At these low pressures the titanium atoms appear to be unaffected by the oxygen background gas, similar to the 1D simulations, due to the limited number of collisions. The spatial spreading is much larger in the oxygen part of the plume than the titanium part. This is because the oxygen part of the plasma plume has a higher initial velocity than the titanium part. The angular spread remains the same, since it was assumed to be the same for both Ti and O. After $3 \mu\text{s}$ the first oxygen particles already arrive at the substrate surface for a low oxygen background pressure of 0.02 mbar. This could significantly influence the oxidation state of the substrate surface before arrival of the slower titanium particles.

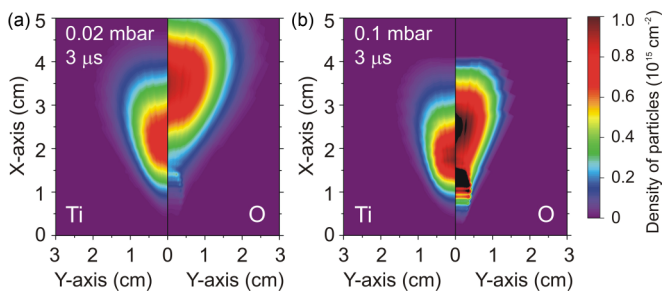


FIG. 8. 3D simulations of the plasma plume propagation exhibiting the densities of Ti and O particles, integrated over the direction normal to the figure, at $3 \mu\text{s}$ after ablation for oxygen background pressures of (a) 0.02 and (b) 0.1 mbar.

At a higher pressure of 0.1 mbar the plasma behaves differently as compared to the low-pressure propagation. The Ti part of the plume is not as wide as for the low-pressure propagation (although the angular spread is the same) caused by slowdown of the plume due to collisions with the oxygen background gas. The plume is therefore more compressed and has a higher density. The 3D simulations confirm the dramatic drop in kinetic energy of the oxygen particles within the plasma plume as shown already in the 1D simulations. The large number of collisions with the oxygen background gas at 0.1 mbar leads to a large decrease in velocity of the low-mass O particles. Already after $3 \mu\text{s}$ the simulations indicate that a large amount of O particles has almost come to a standstill 1–2 cm away from the ablated area on the target. In the model this is atomic oxygen, which has collided elastically with oxygen molecules, since no chemical reactions were assumed to take place. In practice we expect that ozone may be formed which on further collisions decomposes in O_2 . The oxygen pressure buildup in the 1–3 cm region by these very slow molecules should drop over longer timescales by self-diffusion, which is not modeled here.

C. Oxidation state of particles in plasma

Enhanced control of thin-film growth requires a detailed understanding of the specific oxidation state and kinetic energy of the arriving particles. Several possible sources of oxygen (target, background gas, substrate) can contribute to the oxidation process during pulsed laser deposition of oxide thin films. The effect of oxygen in the target and/or background gas depends strongly on the applied pressure, while oxygen release from an oxide substrate is mostly negligible. The oxidation of the particles in a plasma plume ablated from a TiO_2 target was measured by spectral analysis of the self-emission of the plume under different deposition conditions

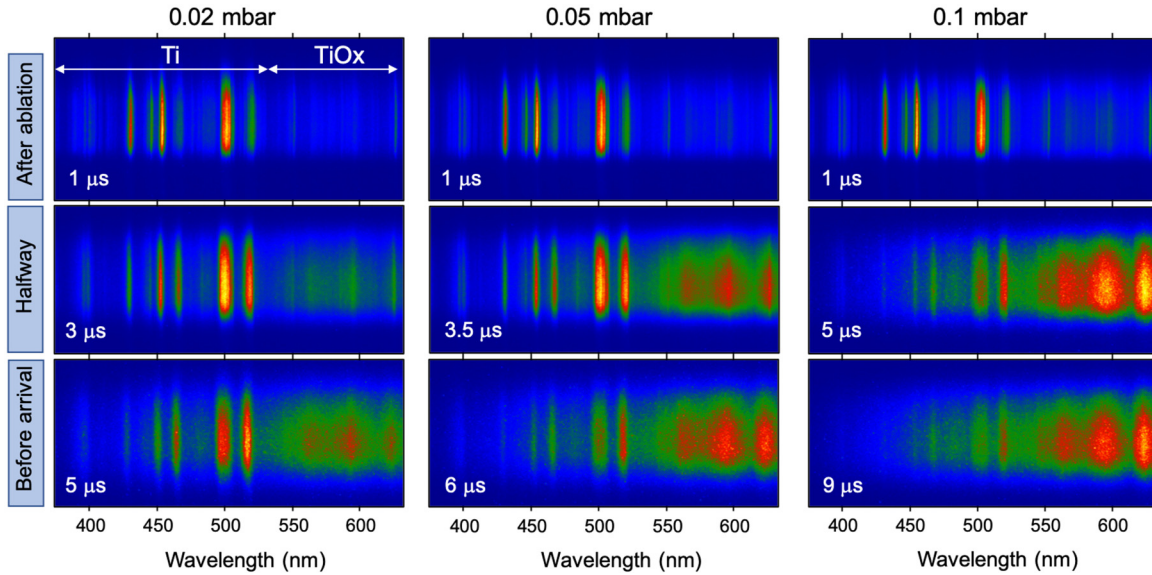


FIG. 9. Time-resolved optical emission spectroscopy of a PLD plume ablated from a TiO₂ target at oxygen pressures of 0.02, 0.05, and 0.1 mbar. Spectra are shown for different time intervals (in μs), corresponding to propagation distances shortly after ablation from the target, halfway between target and substrate, and directly before arrival on the substrate.

with variable oxygen pressures, see Fig. 9. Spectra are shown for different time intervals, corresponding to propagation distances shortly after ablation from the target, halfway between the target and substrate, and directly before deposition on the substrate.

For all pressures (0.02, 0.05, and 0.1 mbar) similar spectra can be observed directly after ablation of the target, indicating the formation of oxygen and titanium particles. Self-emission of the oxygen particles is three orders of magnitude weaker than self-emission of the titanium particles [22] and therefore cannot be distinguished in the spectra. During subsequent propagation of the particles away from the target, the titanium particles undergo collisions with the oxygen particles, which results in the formation of TiO particles. This can be seen in the spectra by the enhanced intensities at the longer wavelengths. As discussed above, the number of collisions depends strongly on the background pressure, which is confirmed by the experimental spectra in Fig. 9 halfway between target and substrate, showing enhanced TiO formation at higher oxygen pressures. This oxidation process continues until the particles arrive at the substrate surface. It can be seen in Fig. 9 that for a low oxygen pressure of 0.02 mbar the plasma plume did not fully transform into TiO particles and a significant amount of nonoxidized Ti particles will contribute in the thin-film growth. For a higher oxygen pressure of 0.05 mbar the intensities of the TiO spectral lines increase, while the intensity of the Ti spectral lines decreases significantly. This oxidation process becomes even clearer for a high oxygen pressure of 0.1 mbar in which the intensity of the Ti spectral lines reduces further, and TiO particles form the majority when arriving at the substrate surface. These results are consistent with previous experimental studies of the plasma plume oxidation during SrTiO₃ growth [4,7].

The oxidation of the particles in the plasma plume have been modeled by adding the chemical reactions during each collision. The conditions for formation of a metal-oxide parti-

cle are satisfied when a collision between a metal atom (*M*) and an oxygen atom (*O*) occurs. The collision conditions are such that initially *M*₁*O*₁ is formed before transforming subsequently into the *M*₁*O*₂ state during a second collision.

The accumulation of specific particles arriving at the substrate can be determined from the 3D simulations at *t* = 18 μs after ablation, assuming a typical substrate size of 5 × 5 mm² and placed in the center in front of the plasma plume at a distance of 5 cm. Figure 10 shows the variation in relative amounts of arriving particles when the oxygen background pressure is varied between 0.01 and 0.1 mbar. At 0.01 mbar a large amount of Ti particles arrive nonoxidized on the substrate, while a small fraction has reacted into TiO

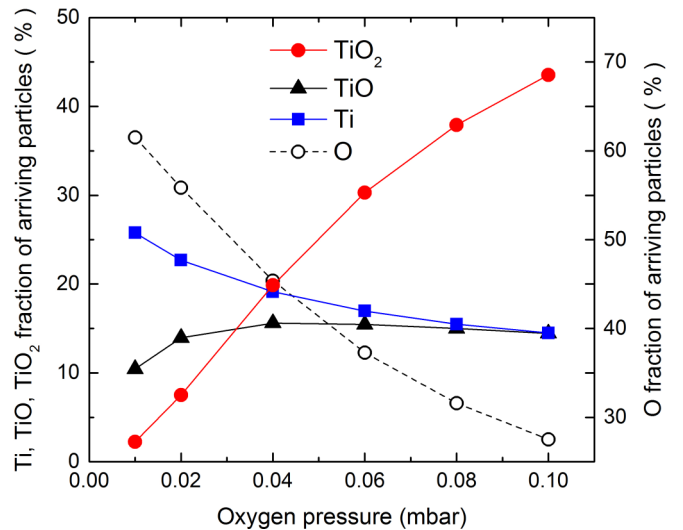


FIG. 10. Simulated results of the accumulated amount of particles and their oxidation state arriving at the substrate 18 μs after TiO₂ ablation for different oxygen pressures.

and almost no TiO_2 is present. This is in good agreement with experimental observations that at low pressures almost no oxidation occurs in the plasma plume. When the pressure increases to 0.02 mbar, some TiO reacts to TiO_2 due to enhanced collisions between TiO and O background particles. Note that a large number of (nonoxidized and oxidized) particles will not contribute to film growth on small substrates with limited dimensions, e.g., $5 \times 5 \text{ mm}^2$, placed on the heart line of the plume, because they end up outside the substrate area due to the angular spreading. The amount of oxygen particles originating from the target arriving at the substrate decreases drastically for higher background pressures caused by the large kinetic energy loss after each collision. Therefore oxidation of the metal atoms in the plasma appears essential to build in sufficient oxygen in the growing film to obtain the desired crystal structure. It was shown that doping with atoms with different valency, as well as incomplete oxidation, of multivalent atoms in Nb-doped Ti oxide films can change the film from an insulator into a transparent conductor [23]. This shows the importance of the oxidation reactions in the plasma, which strongly depend on the background pressure, for the structural and physical properties of the grown film.

However, for increasing pressures above 0.02 mbar, the number of TiO particles stabilizes, whereas the amount of Ti atoms arriving at the substrate reaches a plateau of about 15% of the arriving target atoms. Oxidized TiO species are located at the outer edge of the plume and are therefore more likely to collide with the oxygen background gas and transform further into TiO_2 . Experimental measurements also indicate that in the pressure range of 0.02–0.05 mbar the plasma plume propagation changes from a ballistic regime to a diffuse regime. This observation is in good agreement with the simulation results, showing the TiO_2 particles to become the dominant species in the plasma plume. For a high oxygen pressure of 0.1 mbar, the majority of the species arriving at the substrate are oxidized (TiO and TiO_2). They exhibit a reduced kinetic energy as compared to lower pressures, which can also be observed in the reduced intensities of the self-emission intensities directly before deposition on the substrate, Fig. 9.

D. Lateral variations of deposited particles

The three-dimensional nature of our numerical model enables us to simulate the lateral variations in deposited particles on the substrate surface, which could cause local differences in the composition of the grown thin film. High-quality thin films with homogeneous properties over the complete surface area require the composition to be absolutely constant. Scientific studies by pulsed laser deposition in research laboratories are normally limited to sample dimensions up to diameters of about 1 cm. Upscaling pulsed laser deposition to larger dimensions for industrial applications have been realized, but complex procedures are required to obtain high-quality coverage [24]. Detailed insight into the expected lateral variations for the deposition of complex oxide materials in different oxygen environments would provide important input for optimizing large-area PLD synthesis.

Figure 11 shows the $\text{Ti}:\text{TiO}$ and $\text{Ti}:\text{TiO}_2$ ratios of the deposited particles on the substrate surface accumulated up to 18 μs after ablation from the TiO_2 target. This time period is suf-

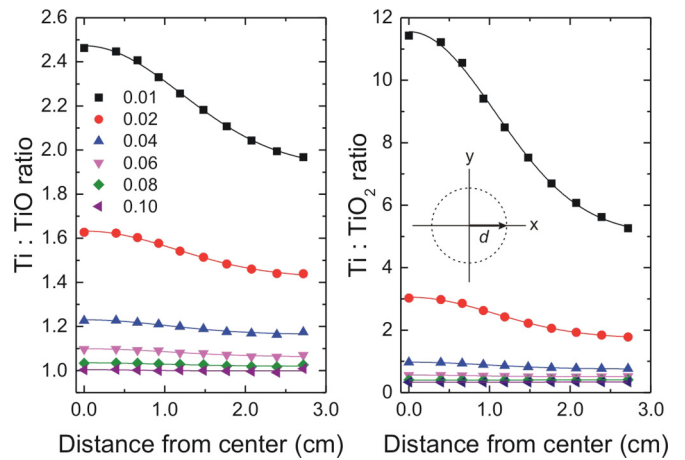


FIG. 11. Simulated results of the lateral variations in (left) $\text{Ti}:\text{TiO}$ and (right) $\text{Ti}:\text{TiO}_2$ ratios of deposited particles on the substrate surface for different oxygen background pressures 18 μs after TiO_2 ablation. The lines are Gaussian distributions fitted to the simulated data. Inset shows the deposited area as distance (d) from the center.

ficient to collect all ablated particles arriving at the substrate for all different oxygen background pressures. It can clearly be observed that for low oxygen pressures of 0.02 mbar the $\text{Ti}:\text{TiO}$ ratio exhibits a large lateral variation away from the center, which can be fitted with a Gaussian distribution. Although a small sample with $d < 0.5 \text{ cm}$ would result in a homogeneous composition with $\text{Ti}:\text{TiO}$ about 2.45, a large sample with $d > 2.5 \text{ cm}$ would exhibit a large gradient in the composition towards a $\text{Ti}:\text{TiO}$ ratio below 2.0 at the sample edges. This lateral variation diminishes for higher oxygen pressures, reaching a constant $\text{Ti}:\text{TiO}$ ratio of 1.0 over the full surface for 0.1 mbar oxygen under the used PLD parameters. Interestingly, the $\text{Ti}:\text{TiO}_2$ ratio shows an even larger lateral variation for low oxygen pressures of 0.02 mbar, which can be fitted with a Gaussian distribution. The $\text{Ti}:\text{TiO}_2$ ratio varies from about 11.5 for a small sample with $d < 0.5 \text{ cm}$ to about 5.0 for a large sample with $d > 2.5 \text{ cm}$. Also, here it can be seen that the lateral variation becomes negligible for higher oxygen pressures, reaching a constant $\text{Ti}:\text{TiO}_2$ ratio of 0.33 over the full surface for 0.1-mbar oxygen under the used PLD parameters.

The enhanced contribution of Ti particles in the center of the deposited area for low oxygen pressures of 0.02 mbar agrees well with our previous observations of titanium particles in the plasma plume propagating towards the substrate. At low oxygen pressures the titanium particles appear to be unaffected by the oxygen background gas due to the limited collisions, as are the oxygen particles, originating from the target, that quickly speed ahead of the Ti plume. Note that since there is no angular spreading assumed to be present during the plume propagation and the same angular spread is assumed for the Ti and O atoms, as described by the n -parameter in Eq. (2), we see qualitatively the same angular distributions in Figs. 8(a) and 8(b). However, the shape and position of, especially at the front of the plume changes due to collisions with the background gas, changing the density of the plume for the different elements at the same observation time. This in turn

changes the chemical interaction rates in the plume, which is significantly enhanced for the high-background-pressure plume, as is also evident from Fig. 11. At high oxygen pressures the widths of the titanium and oxygen parts of the plume are very similar [Fig. 8(b)], leading to a reduced lateral variation. Furthermore, the oxidation of the Ti part of the plume into TiO and TiO₂ particles is significantly enhanced by the increased number of collisions with the oxygen background gas.

The stoichiometry and oxidation state of the arriving particles is only one part of the problem of understanding the growth of oxide thin films. In the experiments we used a single-crystal target to avoid the ablation of material clusters that can be incorporated into growing films, causing growth defects. The type of substrate material and the lattice mismatch at deposition temperatures between the substrate and the film both affect the sticking and surface diffusion of the arriving particles and in this way strongly influence the growth of the film, especially the possible development of grain boundaries. These aspects fall outside the scope of this study but are also important to be investigated further to obtain a better understanding of PLD growth of thin films.

IV. CONCLUSION

The propagation and oxidation of the plasma plume during pulsed laser deposition of TiO₂ was investigated by combining experimental observations with numerical modeling. A more generalized particle scattering model was proposed beyond previous analytical models to simulate the energy, location, and oxidation state of the different types of particles in the PLD plasma plume. The model only contains two fit parameters, which were obtained from fitting the initial shape of the plume. All other parameters were obtained from an energy balance of the laser pulse–target interaction. Comparison between the simulations and the self-emission measurements of the TiO₂ plasma plume showed good agreement, although

small deviations can be explained by differences in the initial velocity distribution. Furthermore, the possibility of a temperature gradient in the background gas was not included in the model. Our model enables a detailed simulation of the oxidation state of the arriving particles (Ti, TiO, and TiO₂) on the substrate surface depending on oxygen background pressure. Comparison of the model with experimental results indicates that oxidation in the plasma takes place only for slow metal plume atoms, and hence after one or several collisions with the background gas. Interestingly, low pressures of about 0.02 mbar result in fast oxygen particles arriving prior to the slower titanium particles, which could significantly influence the oxidation state of the initial substrate surface. The enhanced number of collisions for higher pressures of about 0.1 mbar lead to a large amount of the low-mass oxygen particles coming to a standstill 1–2 cm away from the ablated target.

Furthermore, the 3D nature of our model has enabled simulation of the lateral variations in composition of the deposited particles on the substrate surface. Although negligible variations in the Ti:TiO and Ti:TiO₂ ratios are present for high pressures over deposition areas with diameters up to 5 cm, significant variations can be observed for low pressures. These insights could play an important role in upscaling pulsed laser deposition from a scientific laboratory-based scale to an industrial large-area scale. Finally, the model can be expanded by the addition of a second (or more) metal element, which makes it possible to simulate thin-film growth of more complex oxides with a wide variety of interesting functional properties.

ACKNOWLEDGMENT

This research was supported by the European Commission under FP7-ENERGY-2012-FET, 309018, “AllOxidePV: Novel Composite Oxides by Combinatorial Material Synthesis for Next Generation All-Oxide-Photovoltaics.”

-
- [1] *Epitaxial Growth of Complex Metal Oxides*, edited by G. Koster, M. Huijben, and G. Rijnders (Woodhead Publishing, Sawston, Cambridge, UK, 2015).
 - [2] D. Dijkkamp, T. Venkatesan, X. D. Wu, S. A. Shaheen, N. Jisrawi, Y. H. Min-Lee, W. L. McLean, and M. Croft, *Appl. Phys. Lett.* **51**, 619 (1987).
 - [3] K. Orsel, R. Groenen, H. Bastiaens, G. Koster, G. Rijnders, and K.-J. Boller, *J. Instrum.* **8**, C10021 (2013).
 - [4] K. Orsel, H. Bastiaens, R. Groenen, G. Koster, A. Rijnders, and K.-J. Boller, *APL Mater.* **3**, 106103 (2015).
 - [5] S. Amoruso, A. Sambri, and X. Wang, *J. Appl. Phys.* **100**, 013302 (2006).
 - [6] S. Wicklein, A. Sambri, S. Amoruso, X. Wang, R. Bruzzese, A. Koehl, and R. Dittmann, *Appl. Phys. Lett.* **101**, 131601 (2012).
 - [7] R. Groenen, J. Smit, K. Orsel, A. Vailionis, B. Bastiaens, M. Huijben, K. Boller, G. Rijnders, and G. Koster, *APL Mater.* **3**, 070701 (2015).
 - [8] *Physics of Shock Waves and High Temperature Hydrodynamic Phenomena*, edited by Y. B. Zeldovich and Y. P. Raizer (Academic Press, New York, 1966).
 - [9] D. B. Geohegan, *Appl. Phys. Lett.* **60**, 2732 (1992).
 - [10] M. Strikovski and J. H. J. Miller, *Appl. Phys. Lett.* **73**, 1733 (1998).
 - [11] J. Gonzalo, C. N. Afonso, and I. Madariaga, *J. Appl. Phys.* **81**, 951 (1997).
 - [12] R. Wood, J. Leboeuf, K. Chen, D. Geohegan, and A. Puzos, *Appl. Surf. Sci.* **127-129**, 151 (1998).
 - [13] R. F. Wood, J. N. Leboeuf, D. B. Geohegan, A. A. Puzos, and K. R. Chen, *Phys. Rev. B* **58**, 1533 (1998).
 - [14] S. S. Mao, X. Mao, R. Greif, and R. E. Russo, *Appl. Phys. Lett.* **77**, 2464 (2000).
 - [15] H. Long, G. Yang, A. Chen, Y. Li, and P. Lu, *Thin Solid Films* **217**, 745 (2008).
 - [16] D. A. H. Hanaor and C. C. Sorrell, *J. Mater. Sci.* **46**, 855 (2011).

- [17] See Supplemental Material at <http://link.aps.org/supplemental/10.1103/PhysRevMaterials.4.103803> for the exposure time and gain settings of the camera for the different self-emission measurements.
- [18] *Pulsed Laser Deposition of Thin Films*, edited by D. Chrisey and G. Hubler (John Wiley and Sons, New York, 1994).
- [19] K. K. Anoop, S. S. Harilal, R. Philip, R. Bruzzese, and S. Amoruso, *J. Appl. Phys.* **120**, 185901 (2016).
- [20] *Bond Energies in Oxide Systems: Calculated and Experimental Data*, edited by V. Stolyarova, E. Plotnikov, and S. Lopatin (John Wiley and Sons, New York, 2003).
- [21] L. Doeswijk, G. Rijnders, and D. Blank, *Appl. Phys. A* **78**, 263 (2004).
- [22] A. Kramida, Y. Ralchenko, and J. Reader, NIST Atomic Spectra Database (ver. 5.7.1) (2019).
- [23] Y. Furubayashi, T. Hitosugi, Y. Yamamoto, K. Inaba, G. Kinoda, Y. Hirose, T. Shimada, and T. Hasegawa, *Appl. Phys. Lett.* **86**, 252101 (2005).
- [24] D. H. A. Blank, M. Dekkers, and G. Rijnders, *J. Phys. D: Appl. Phys.* **47**, 034006 (2014).